The Crystallization of Mercury's Magma Ocean and the Influence of Sulfur on the Evolution of the Innermost Planet

Fabrizio Saracino
Department of Geology, University of Liège, Allée du Six Août 14, 4000 Liège
DOI: 10.19276/plinius.2026.01.018

INTRODUCTION

Accretionary impacts, metal–silicate segregation, and the decay of short-lived radioisotopes would have produced enough heat to completely melt Mercury in its early history, forming a vast silicate magma ocean (Charlier & Namur, 2019). Subsequent crystallization of the magma ocean eventually produced the primordial Mercurian mantle, whose structure was determined by the crystallization regime and the initial composition of bulk silicate Mercury (BSMe), although the latter remains debated (Fischer & Parman, 2025). Several experimental studies hint at a significant compositional diversity within Mercury's mantle (Namur et al., 2016). Partial melting of specific chondritic precursors could also generate a variety of lava compositions, but this process alone cannot account for the full range of surface compositions observed on Mercury (Boujibar et al., 2025). Investigating the crystallization products of Mercury's magma ocean (MMO) is thus crucial as its initial structure would have affected the thermal evolution of the mantle, setting the stage for mantle melt generation and effusive volcanism, which built the secondary crust until ca. 3.5 Ga (Byrne et al., 2016). The MMO was unique among the terrestrial planets: NASA's MESSENGER spacecraft indeed revealed the unusually high sulfur content and near FeO-free nature of Mercury's lavas, which indicate highly reduced conditions of formation (Zolotov et al., 2013). The high inferred bulk mantle S content (Lark et al., 2022) has led authors to suggest that sulfides should have formed in the MMO. These would have been sequestered in the mantle and/or primordial crust and potentially stored heat-producing elements (HPEs; Boukaré et al., 2019). Vander Kaaden and McCubbin (2015) suggested that graphite would have been the only buoyant phase in such a FeO-poor MMO, which would have likely contributed to the formation of a C-rich primordial crust. Investigating melt density and the effect of sulfur in the evolving magma ocean proves therefore crucial to quantitatively evaluate if other light phases (sulfides, quartz, and plagioclase) could have become buoyant during solidification. Moreover, if containing significant amounts of HPEs, the distribution of sulfide phases could have substantially impacted Mercury's thermal evolution (Boujibar et al., 2019).

The goal of this study is to investigate the structure of the primordial mantle of Mercury as the direct result of the crystallization of its magma ocean. Starting from phase equilibria experiments, we develop a crystallization model of the mineralogical and chemical evolution of the MMO for a range of BSMe starting compositions. In parallel, we investigate the role of sulfur on the differentiation and density of silicate residual liquids, coupled with the probability of crystal flotation and its impact on the distribution of HPEs. This study provides a revised standard model for the evolution of planet Mercury in its early turbulent history.

METHODS

Bulk Silicate Mercury

Primitive meteorites like enstatite chondrites (ECs) have commonly been considered as good analogs of Mercury's building blocks owing to their similar geochemical signatures, including FeO-depleted silicate phases and high abundances of sulfur and alkali metals (Na, K; Nittler et al., 2018). BSMe compositions have been investigated either by defining magmatic fractionation lines of surface and mantle compositions (*e.g.*, Anzures et al., 2020), or by combining surface measurements with laboratory experiments simulating mantle melting (Namur et al., 2016). In this work, the BSMe compositions are inspired by the silicate fraction of ECs (Table 1; Xu et al., 2024; Saracino et al., 2025). An average composition was obtained from analyses of both high-iron (EH) and low-iron (EL) ECs (Jarosewich, 1990; Berthet et al., 2009). The P_2O_5 content was decreased to account for the markedly siderophile behaviour of P (Gu et al., 2019). Si was also partly removed from the original chondritic materials: two compositions with different Mg/Si ratios were selected, which correspond to the segregation of 8 wt.% and 15 wt.% Si from the silicate portion into the metallic core (named Mer8 and Mer15, respectively). Considering that Mercury's core represents 67% of the planet's mass (Hauck et al., 2013), these values reflect core Si abundances of 2.9 wt.% (Mer8) and 5.5 wt.% Si (Mer15). These values span the lower range of Si estimates in the core of Mercury (Nittler et al., 2018). Testing

Table 1 Composition of starting materials.

	Mer8	Mer15	Mer_1	Mer_2	Mer_3
SiO_2	54.82	47.91	56.53	62.91	66.48
TiO_2	0.14	0.16	0.38	0.17	0.16
Al_2O_3	3.70	4.26	9.46	13.85	16.62
Cr_2O_3	0.52	0.60	0.56	0.11	0.02
MnO	0.28	0.33	0.37	0.31	0.04
MgO	37.32	43.04	24.01	11.95	4.39
CaO	1.62	1.87	4.33	5.12	5.68
Na_2O	1.37	1.58	3.75	5.10	6.00
K_2O	0.13	0.15	0.36	0.49	0.60
P_2O_5	0.10	0.10	0.26	n.d.	n.d.
Total	100.00	100.00	100.00	100.00	100.00

starting compositions with a range of different Mg/Si ratios is crucial as Mg/Si is known to promote the stability of either enstatite or forsterite (Namur et al., 2016).

Modelling strategy

We follow the modelling strategy of Elkins-Tanton et al. (2003) and Charlier et al. (2018), who developed a code to simulate the fractional crystallization of the Martian and lunar magma oceans, respectively. Our code is grounded in experimentally determined phase equilibria and traces the solidification steps of the MMO through a stepwise approach in which we calculate the mineralogy, composition, and density of cumulates while tracking the compositional evolution of the residual silicate liquids. The initial compositions of the silicate liquid are the primitive compositions Mer8 and Mer15. Major elements and heat-producing elements (U, Th, K) were considered. FeO was ignored because MESSENGER data have demonstrated the paucity of FeO on the surface (Nittler et al., 2018). The initial depth of the MMO was calculated using gravity models for Mercury (Goossens et al., 2022). We simulate the crystallization of the MMO from an initial depth of ~480 km, corresponding to the maximum possible core-mantle boundary (CMB) depth. Accordingly, we account for a higher volume of the silicate magma ocean, which is considered to have been ca. 17% greater than the present-day solid silicate shell.

Importantly, literature data on near-liquidus experiments representative of the BSMe provide precious insights into the phase equilibria of early forming minerals segregating from the MMO (Xu et al., 2024; Saracino et al., 2025). Xu et al. (2024) and Saracino et al. (2025) showed that enstatite is the liquidus phase in sulfide-saturated Mer8 whereas forsterite is the liquidus phase in sulfide-saturated Mer15 between 1 and 7 GPa. Saracino et al. (2025) showed that the residual melt compositions of sulfide-saturated Mer8 and Mer15 converge, eventually reaching a single cotectic curve after sufficient differentiation. The initial fractionation of the MMO can therefore be simulated by fractionating only enstatite for Mer8 and only forsterite for Mer15 until the residual MMO liquids reach the forsterite-enstatite cotectic. After reaching this cotectic curve, all Mercurian melts, including low- and high-Mg/Si melts, evolve towards the same eutectic where crystallization ends (Namur & Charlier, 2017). Accordingly, during the first stage of crystallization, the Mg/Si ratios of the Mer8 and Mer15 residual liquids converge. To further evolve the MMO, we consider an average of the two residual liquid compositions.

Experimental strategy

Low-to-high pressure (0.5–3.0 GPa) and high temperature (1125–1950°C) experiments were designed to simulate the evolution of the silicate MMO liquid during cooling as crystallization proceeds, while melt fraction (F) decreases. The first experimental series was performed on compositions representative of BSMe (Mer8 and Mer15), in order to study the effects of S on the liquidus temperature and silicate phase equilibria of reduced primitive melts. We then simulated enstatite and forsterite fractionation from Mer8 and Mer15, respectively, until the two residual liquids converged chemically. We name this residual liquid composition Mer_1 (Table 1), which corresponds to the cotectic composition at which enstatite and forsterite coexist, following the crystallization of enstatite from Mer8 and forsterite from Mer15 using the forward crystallization model described above. Experiments on Mer_1 were performed until clinopyroxene joined the mineral assemblage with forsterite and enstatite. We then used the new residual melt composition in equilibrium with clinopyroxene, Mer_2 (Table 1), in further experiments until the appearance of quartz, which also corresponded to the destabilization of forsterite due to the high activity of SiO_2.

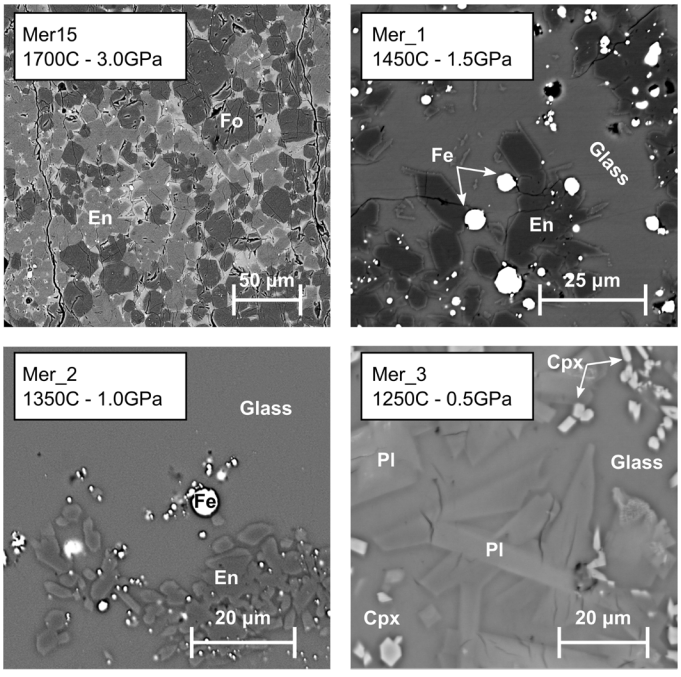

Figure 1 Representative BSE images of experimental products. En – Enstatite, Fo – Forsterite, Cpx – Clinopyroxene, Pl – Plagioclase, Fe – Fe metal.

Lastly, a final composition produced from the Mer_2 residual melts, Mer_3 (Table 1), was used to attain the most evolved stages of magma ocean solidification.

Experiments were conducted with a Voggenreiter Mavo LPC 250-300/50 end-loaded piston-cylinder apparatus at the University of Liège (Belgium). 1/2″ assemblies were used in the pressure range 1.0–3.0 GPa, and 3/4″ assemblies for runs at 0.5 GPa. For the 1/2″ assembly, a graphite capsule with a MgO spacer was placed in a graphite furnace, and a $BaCO_3$ cell was used as the pressure medium. In the 3/4″ assembly, a talc + pyrex cylinder was used as the pressure medium. Temperature was monitored with a D-type thermocouple for both assemblies. The assemblies were first pressurized at room temperature to 0.7 GPa in the 1/2″ setup and 0.4 GPa in the 3/4″ setup. Then, temperature was increased to 865°C at 100°C/min while keeping the pressure constant. Temperature was then held for 6 min to pressurize to the target pressure. Finally, temperature was increased again at 50°C/min until the target temperature was attained. Experiments were quenched by switching off the power. Upon extraction, the experimental samples were cut in half using a diamond wafer saw, mounted in epoxy, and ultimately polished with an alcohol-based polycrystalline 1 µm diamond suspension preserving all sulfides.

Analytical strategy

Sample characterization was performed through non-destructive qualitative and quantitative analytical techniques. Qualitative analysis of our samples, including imaging and phase identification, was performed with the FEI QEMSCAN at RWTH Aachen (Germany), and with the TESCAN MIRA (4th Gen) at the Department of Geology at KU Leuven (Belgium). Quantitative analyses were performed by employing the CAMECA SX Five Tactis at Laboratoire Magmas et Volcans, Université Clermont Auvergne (Clermont-Ferrand, France), and with the JEOL JXA-8530F at the Department of Materials Engineering at KU Leuven (Belgium). Both natural and synthetic standards were used for EPMA calibration. More details on the EPMA standards and settings are in Saracino et al. (2025, 2026).

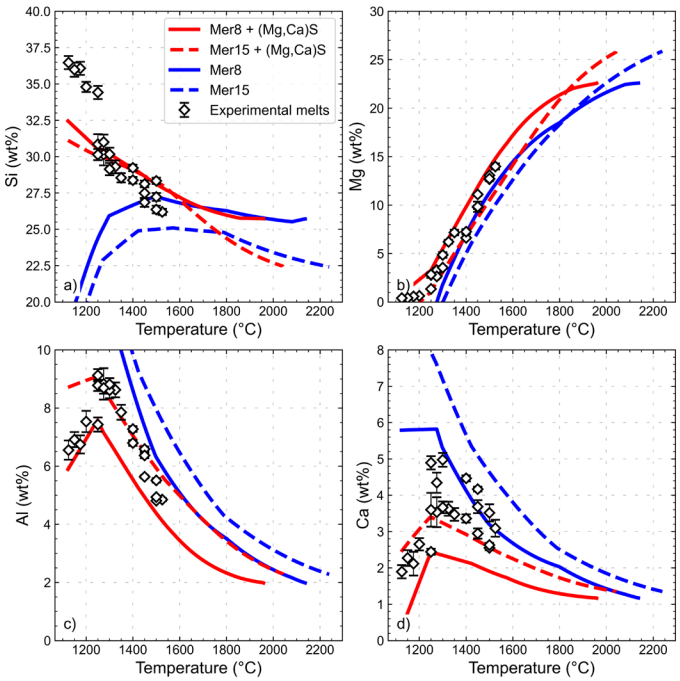

Figure 2 Comparison between modelled MMO liquids and experimental melts.

RESULTS

Phase equilibria and composition of silicate phases

Representative back-scattered images of the experiments are shown in Figure 1. Enstatite is the liquidus phase in Mer8, whereas forsterite is the liquidus phase in Mer15 (Saracino et al., 2025). With progressive crystallization, the residual liquids of both compositions reach the enstatite-forsterite cotectic (Fig. 2). Clinopyroxene later joins the forsterite-enstatite assemblage at 1500°C (Mer_1), followed by quartz at 1400°C. Forsterite becomes unstable below 1275°C (Mer_2) while enstatite destabilizes below 1250°C. This temperature also marks the first appearance of plagioclase (Mer_3; Fig. 1). Experimental liquid lines of descent (LLDs) obtained after the fractionation of early forming minerals for both Mer8 and Mer15 are presented in Figure 2. The Si content constantly increased (26–37 wt.%, Fig. 2a) from 1550 to 1100°C, whereas the Mg content steadily dropped (15–0 wt.%) (Fig. 2b). Na was also progressively enriched in the glass (1–6 wt.%) with decreasing temperature. S content decreased from 1550 to 1250°C (no S was added to experiments run at < 1250°C). Both Al and Ca were enriched in the glass from 1550 to 1250°C, but were then depleted at lower temperatures (Fig. 2c,d) due to the saturation of plagioclase and clinopyroxene. In all experiments, olivine and orthopyroxene matched their Mg endmember compositions (forsterite and enstatite, respectively). We only observed increasing CaO and Al_2O_3 contents in the enstatite composition over the range of starting materials investigated. Clinopyroxene is mostly diopsidic, whereas plagioclase becomes increasingly albitic with decreasing temperature.

MMO parameterization

The experimentally determined phase relations were used to mimic the fractional crystallization of the MMO. We calculated the cotectic proportions of mineral phases in order to model melt differentiation consistent with the experimental LLDs. We used temperature as the main criterion to define the saturation or the destabilization of solid phases in the growing cumulate pile. We developed a S-free liquid thermometer based on experimental studies of Mercury-like mantle compositions (Saracino et al., 2025). Here we applied a correction ($\Delta T_{Liquidus} = T_{Liquidus,S\text{-}free} - T_{Liquidus,S\text{-}bearing}$) to account for the depression of the liquidus temperature in the presence of sulfur (Fig. 3). The densities of crystals in the cu-

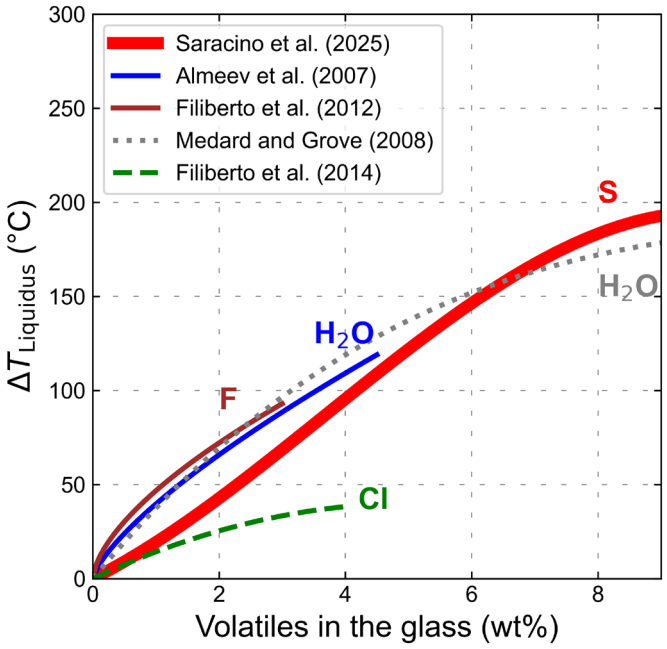

Figure 3 The effect of S on the liquidus temperature of reduced Mg-rich melts.

mulate pile were determined at the solidus temperature derived by fitting the solidi of the evolving MMO liquid as determined using MAGEMin (Riel et al., 2022). The effects of temperature and pressure on mineral densities were calculated with a third-order Birch-Murnaghan EoS.

DISCUSSION

MMO evolution and cumulate pile lithology

The evolution of the modelled MMO liquids for both Mer8 and Mer15 and a comparison with the experimental melts are reported in Figure 2. The crystallization sequence of Mer8 and Mer15 as MMO bulk compositions is shown in Figure 4 as a function of depth. In Mer8, the MMO solidification starts with the formation of a ~90-km-thick basal enstatite layer, whereas Mer15 forms a ~300-km-thick dunitic basal layer (Fig. 4a). The residual melt of Mer8 becomes co-saturated in forsterite and enstatite at F = 0.81, whereas Mer15 reaches the forsterite-enstatite cotectic at F = 0.38. A thick dunite layer in Mer15 is produced before the MMO residual liquid saturates enstatite too (Fig. 4b). Here, the compositions of the residual melts from Mer8 and Mer15 become similar. Over this range of F (1.00–0.81 for Mer8 and 1.00–0.38 for Mer15), Si, Al, and Ca contents increase in the melt, and the Mg content decreases due to the formation of enstatite and/or forsterite (Fig. 2). Clinopyroxene is the next phase to appear at F = 0.40 in Mer8 and F = 0.35 in Mer15. Forsterite-enstatite-clinopyroxene assemblages are then followed by the appearance of quartz at F = 0.24 in Mer8 and at F = 0.28 in Mer15. Forsterite is stable until F = 0.15 in Mer8 and until F = 0.21 in Mer15, after which it disappears. Plagioclase finally crystallizes at F = 0.14 in Mer8 and F = 0.19 in Mer15, when enstatite becomes unstable. The formation of plagioclase is accompanied by a depletion of both Ca and Al in the residual liquids of both Mer8 and Mer15 (Fig. 2).

Refractory and fertile mantle reservoirs on Mercury

Our results show that a refractory mantle is produced in the lower cumulate pile, which could be uniquely forsterite, uniquely enstatite, or include both phases. In the upper-MMO sequence, a fertile mantle forms when clinopyroxene becomes part of the cumulus assemblage. Experimental studies have shown that a refractory mantle made of an olivine + orthopyroxene assemblage would melt congruently between 1680°C at 1.2 GPa and 1780°C at 2.5 GPa (Chen & Presnall, 1975). Conversely, a mantle containing olivine + orthopyroxene + clinopy-

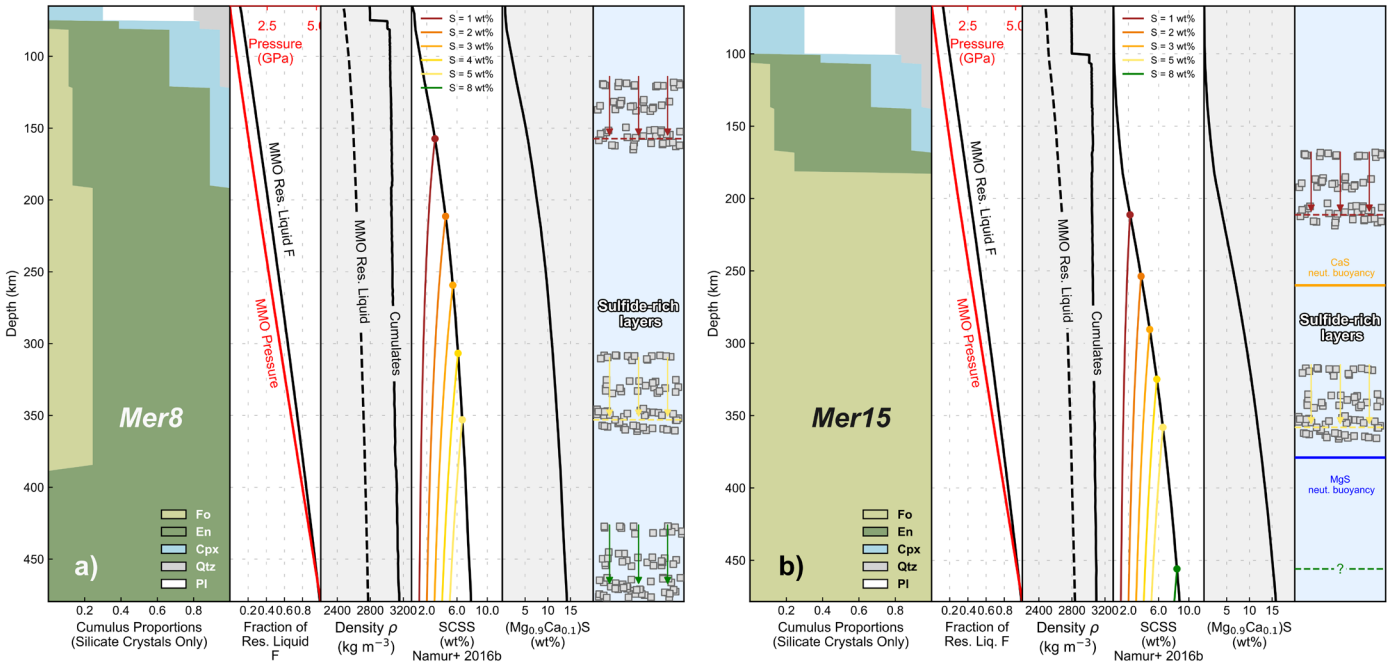

Figure 4 Crystallization sequence of S-bearing **a)** Mer8 and **b)** Mer15 as a function of depth (km). Also shown are the variation of melt fraction, density, sulfur concentration and corresponding sulfide content a function of depth.

roxene would start melting between 1310–1320°C at 1.2 GPa and 1520°C at 2.5 GPa (Walter & Presnall, 1994). Because of the contrasting fusibility of the refractory and fertile mantles, it is expected that the fertile mantle was the dominant contributor to crustal production via partial melting. Here, we evaluate whether the fertile mantle produced by MMO crystallization can actually produce the relatively thick volcanic surface of Mercury by partial melting alone. We consider the thickness of the fertile mantle to be ~140 km. We then calculate the volume of the silicate shell corresponding to the fertile reservoir. From this, we can calculate the volume of melt produced at a fixed melt fraction F, and the relative thickness it would produce as lavas after extraction and cooling at the surface. We first consider a minimum degree of partial melting (F = 0.30) among estimated values in the literature (Namur et al., 2016; Beuthe et al., 2020; Wang et al., 2022; Boujibar et al., 2025). Then we can calculate the volume of partial melt produced, and therefore the thickness of the layer that such a melt would produce at the surface (or within the crust; i.e. intrusive magmatism). We find the thickness of the volcanic crust to be 40 km, in good agreement with the estimated crustal thickness of 35 ± 17 km of Padovan et al. (2015). Higher degrees of partial melting have also been suggested (Boujibar et al., 2025), which would indeed yield a crustal thickness in the range 60–80 km. The range of crustal thicknesses produced by low degrees of partial melting is well within the various estimates of the extent of the Mercurian crust (Padovan et al., 2015). Our results therefore suggest that Mercury's volcanic crust may have originated from the partial melting of the fertile mantle portion alone.

MMO density and the potential for mineral flotation

Determining the density of silicate melts containing sulfur requires knowledge of the nature of bonding between S and typical silicate melt cations, for which the uncertainties remain large. Silicate melts are considered to dissolve ionic S (*e.g.*, O'Neill, 2021), although several studies have demonstrated the bonding of S with cations like Mg, Ca, Si, and Na in silicate glasses using a variety of analytical approaches (Anzures et al., 2020; Pommier et al., 2023). If we assume MgS and CaS as melt species in sulfur-bearing silicate melts, the bonding of S with Mg and Ca would decrease the activities, and therefore the molar fractions, of MgO and CaO species in the silicate melt, which have higher specific densities (3300–3600 kg m^{-3}) compared to S and other sulfides. Furthermore, the occurrence of MgS and CaS melt species will increase, which have specific densities of ~2500–2700 kg m^{-3} in their solid form (Lark et al., 2022). The densities of these species are higher than dominant melt components like SiO_2 (2200 kg m^{-3}) but lower than the specific densities of MgO and CaO. The densities of silicate liquids containing dissolved S should, in principle, slightly decrease. We therefore calculated the effect of sulfur on the density of the MMO liquid (details are in Saracino et al., 2026). The resulting densities of the MMO calculated for Mer8 and Mer15 both in S-free and S-bearing conditions are shown in Figure 5. To our knowledge, this study is the first attempt to explore the impact of S on the density of reduced, Mg-rich silicate melts. We importantly find that sulfur plays a major role in decreasing the density of silicate liquids. For example, around 10 wt.% S dissolved in a silicate liquid would decrease the density by ca. 210 kg m^{-3}. This effect may have serious consequences on the ability of newly formed solid phases to float in a vast magma ocean. To investigate the possibility that minerals formed in the MMO could become buoyant, we compare the densities of the S-bearing residual liquids for both the Mer8 and Mer15 BSMe compositions with the density of solid phases as a function of depth (Fig. 5). Graphite has a lower density than any residual MMO melt and may have thus continuously contributed to the formation of the primordial graphite crust. Quartz, appearing at F = 0.24–0.28, is denser than the residual melts. We also plot potential sulfide minerals (niningerite, MgS; oldhamite, CaS) that could have segregated from the MMO. For Mer8, since the beginning of MMO crystallization, the density of the MMO liquid is lower than the densities of the sulfides. If the MMO was initially sulfide saturated, we would then expect the sulfides to sink into the cumulate pile with the early formed silicates like enstatite and/or forsterite (last panel in Fig. 4). Even in the case that sulfide saturation was attained later during MMO crystallization, the newly formed sulfides would still have been denser than the residual liquid (Fig. 4). As for Mer15, we observe that at CMB conditions, sulfides are slightly positively buoyant with respect to the MMO liquid ($\Delta\rho_{sulfides,MMO}$ = –3 down to –13 kg m^{-3}). Nonetheless, gravitational phase segregation depends on crystal size (Solomatov, 2015), and sulfide flotation may have been hindered by turbulent convection in the magma ocean (Schmidt &

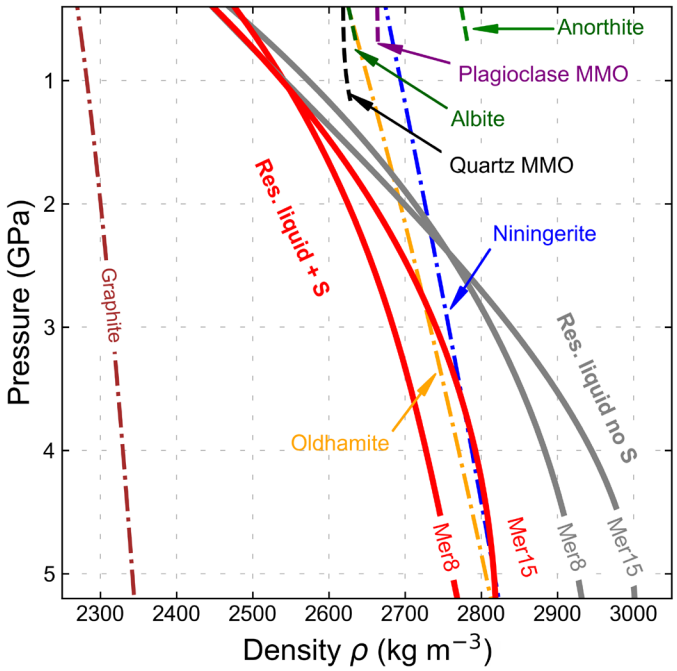

Figure 5 *Densities of evolving MMO liquids as compared to plagioclase, quartz, graphite, and Mg-, Ca-sulfides.*

Kraettli, 2022). In the case of Mer15, the density contrast between the sulfides and the magma ocean is too small to effectively segregate sulfides; in this case, sulfides would be trapped amongst the co-crystallizing forsterite minerals. Considering a MMO of Mer15 composition saturated with sulfides at the onset of crystallization, the sulfides, whether formed before or after the sulfide density crossover, would be stored in the lower and intermediate sections of the mantle. In the alternative case where the MMO Mer15 composition is not saturated with sulfides from the onset of crystallization, sulfides would likely start forming at intermediate depths in the mantle.

Implications for the storage of HPEs

The partitioning of U, Th, K between the silicate, metallic, and sulfide phases may have been influenced by the reduced conditions during Mercury's differentiation (Pirotte et al., 2023). Elements tend to become more chalcophile and siderophile at increasingly reduced conditions (McCubbin et al., 2012). A FeS layer atop the metallic core may also affect the HPE distribution and heat production (Boukaré et al., 2019), although the existence of such a layer remains debated (Pirotte et al., 2023). Oxygen fugacity and the initial S content of the MMO have been shown to affect the storage of U in the Mercurian mantle (Boukaré et al., 2019). Importantly, large uncertainties surround the HPE distribution between Mg-, Ca-sulfides and the silicate melt (*e.g.*, Boukaré et al. 2019). Only Pirotte et al. (2023) recently determined the partition coefficients of HPEs between MgS and the silicate melt under reduced conditions (IW−8.5). Using their estimates, we here quantify HPE partitioning in the MMO for both Mer8 and Mer15 compositions. The concentrations of trace elements, like HPEs, in the MMO are calculated following Rayleigh's equation for fractional crystallization. We calculate the distribution of HPEs based on the estimated (Mg,Ca)S content as shown in Figure 4. Partition coefficients for the silicate minerals are from White (2013). The starting U, Th, and K concentrations in the BSMe are from Pirotte et al. (2023). The concentrations of U, Th, and K in the MMO as a function of depth are reported in Figure 6. For clarity, we only show Mer8. U, Th, and K are all incompatible, and their concentrations increase in the silicate liquid as the cumulate grows in thickness (blue lines in Fig. 6). We also show sulfide-free magma ocean models for comparison (grey lines in Fig. 6). The residual sulfide-bearing liquids are slightly more depleted than the corresponding sulfide-free liquids, given the more compatible behavior displayed by U and Th. Silicate liquids trapped in the growing cumulate might affect the trace element budget of the residual magma ocean liquid (Snyder et al., 1992; Elkins-Tanton et al., 2011). We therefore modelled the HPE budget considering 5% trapped liquid in the cumulate assemblages (orange lines in Fig. 6). HPEs are still enriched in the residual MMO liquid as crystallization proceeds. We

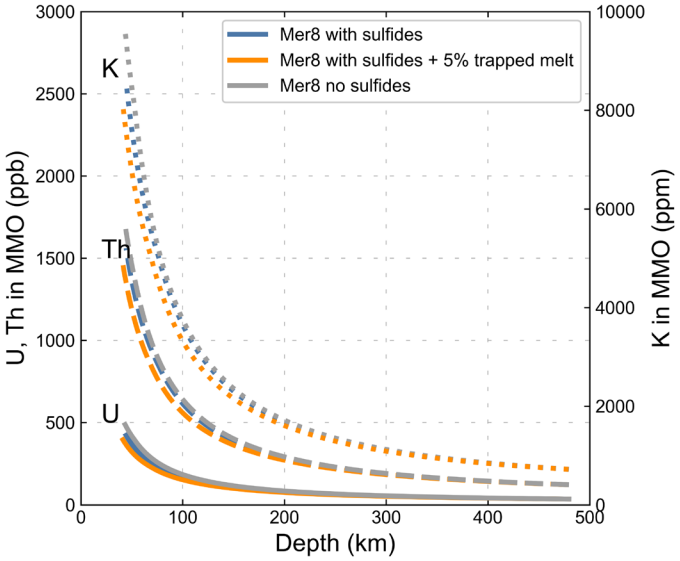

Figure 6 *Uranium, thorium, and potassium distributions in the MMO as a function of depth (km) in Mer8.*

only observe slightly lower HPE abundances compared to sulfide-bearing liquids with no trapped melt. In general, considering both S-free and S-bearing scenarios, we observe that the residual liquid of the MMO would likely contribute to forming a shallow layer that is rich in incompatible elements. A KREEP layer in the upper mantle of Mercury is therefore hypothesized, similar to the Moon (Warren & Wasson, 1979). On Mercury, such a layer would be found between the late cumulates and the primary graphite crust.

CONCLUSIONS

We investigated the crystallization products of a global scale S-rich, reduced magma ocean, in order to reconstruct the structure of the primordial mantle of Mercury. In parallel, we investigated the role of sulfur, such an important element in Mercury's interior, on the phase equilibria, liquidus temperature, liquid density, HPE distribution in a vast range of compositions, oxygen fugacity, and physical conditions.

Our major findings are summarized here below:

- Sulfur strongly impacts phase equilibria. Sulfur promotes the stability of enstatite at the expense of forsterite. It also slightly delays clinopyroxene and plagioclase saturation, while promoting early quartz appearance.
- The lithology of Mercury's primordial mantle relies on BSMe coupled with the presence of S.
- Sulfur is responsible for lowering the liquidus temperature of reduced Mercurian compositions.
- Sulfur plays a crucial role in the MMO chemical evolution. S-free MMO liquids become depleted in silica with progressive crystallization, while S-bearing liquids exhibit enhanced silica enrichment.
- Sulfur also affects the density of the MMO. S-bearing silicate liquids are less dense than S-free liquids.

- Graphite was likely the main mineral to float in the MMO and contributed to the formation of the primordial crust. Sulfide minerals were generally denser than the MMO and were likely stored in the Mercurian mantle.
- HPEs behaved incompatibly in the MMO and likely accumulated in the upper primordial mantle of Mercury. We suggest that a sulfide-bearing KREEP layer, similar to that on the Moon, formed on Mercury.

The upcoming ESA and JAXA BepiColombo mission (Benkhoff et al., 2021) will be able to test our scenarios, therefore providing a revised model of Mercury's internal differentiation and crustal formation. We believe that our study represents a starting point for investigating the early differentiation of Mercury and S-rich exoplanets with high core-to-mantle ratios (Cioria et al., 2024).

REFERENCES

Anzures, B.A., Parman, S.W., Milliken, R.E., Namur, O., Cartier, C., Wang, S. (2020) - Effect of sulfur speciation on chemical and physical properties of very reduced mercurian melts. Geochim. Cosmochim. Acta, 286, 1–18.

Benkhoff, J., Murakami, G., Baumjohann, W., Besse, S., Bunce, E., Casale, M., Cremonese, G., Glassmeier, K.-H., Hayakawa, H., Heyner, D., Hiesinger, H., Huovelin, J., Hussmann, H., Iafolla, V., Iess, L., Kasaba, Y., Kobayashi, M., Milillo, A., Mitrofanov, I.G., Montagnon, E., Novara, M., Orsini, S., Quemerais, E., Reininghaus, U., Saito, Y., Santoli, F., Stramaccioni, D., Sutherland, O., Thomas, N., Yoshikawa, I., Zender, J. (2021) - BepiColombo - mission overview and science goals. Space Sci. Rev., 217, 90.

Berthet, S., Malavergne, V., Righter, K. (2009) - Melting of the Indarch meteorite (EH4 chondrite) at 1GPa and variable oxygen fugacity: implications for early planetary differentiation processes. Geochim. Cosmochim. Acta, 73, 6402–6420.

Beuthe, M., Charlier, B., Namur, O., Rivoldini, A., Van Hoolst, T. (2020) - Mercury's crustal thickness correlates with lateral variations in mantle melt production. Geophys. Res. Lett., 47, e2020GL087261.

Boujibar, A., Habermann, M., Righter, K., Ross, D.K., Pando, K., Righter, M., Chidester, B.A., Danielson, L.R. (2019) - U, Th, and K partitioning between metal, silicate, and sulfide and implications for Mercury's structure, volatile content, and radioactive heat production. Am. Mineral., 104, 1221–1237.

Boujibar, A., Righter, K., Fontaine, E., Collinet, M., Lambart, S., Nittler, L.R., Pando, K.M. (2025) - A pyroxenite mantle on Mercury? Experimental insights from enstatite chondrite melting at pressures up to 5 GPa. Icarus, 437, 116602.

Boukaré, C.-E., Parman, S.W., Parmentier, E.M., Anzures, B.A. (2019) - Production and preservation of sulfide layering in Mercury's mantle. J. Geophys. Res. Planets, 124, 3354–3372.

Byrne, P.K., Ostrach, L.R., Fassett, C.I., Chapman, C.R., Denevi, B.W., Evans, A.J., Klimczak, C., Banks, M.E., Head, J.W., Solomon, S.C. (2016) - Widespread effusive volcanism on Mercury likely ended by about 3.5 Ga. Geophys. Res. Lett., 43, 7408–7416.

Charlier, B., Grove, T.L., Namur, O., Holtz, F. (2018) - Crystallization of the lunar magma ocean and the primordial mantle-crust differentiation of the Moon. Geochim. Cosmochim. Acta, 234, 50–69.

Charlier, B. & Namur, O. (2019) - The origin and differentiation of planet Mercury, Elements 15, 9–14.

Chen, C.-H. & Presnall. D.C. (1975) - The system Mg_2SiO_4-SiO_2 at pressures up to 25 kilobars. Am. Mineral., 60(5-6_Part_1), 398–406.

Cioria, C., Mitri, G., Connolly, J.A.D., Perrillat, J., Saracino, F. (2024) - Mantle mineralogy of reduced sub-Earths exoplanets and exo-Mercuries. J. Geophys. Res. Planets, 129, e2023JE008234.

Elkins-Tanton, L.T, Parmentier, E.M., Hess, P.C., (2003) - Magma ocean fractional crystallization and cumulate overturn in terrestrial planets: Implications for Mars. Meteorit. Planet. Sci., 38(12), 1753–1771.

Fischer, E.L. & Parman, S.W. (2025) - The bulk composition and initial size of Mercury. Icarus, 439, 116664.

Goossens, S., Renaud, J.P., Henning, W.G., Mazarico, E., Bertone, S., Genova, A. (2022) - Evaluation of recent measurements of Mercury's moments of inertia and tides using a comprehensive Markov Chain Monte Carlo method. Planet. Sci. J., 3, 37.

Gu, T., Stagno, V., Fei, Y. (2019) - Partition coefficient of phosphorus between liquid metal and silicate melt with implications for the Martian magma ocean. Phys. Earth Planet. In., 295, 106298.

Hauck, S.A., Margot, J., Solomon, S.C., Phillips, R.J., Johnson, C.L., Lemoine, F.G., Mazarico, E., McCoy, T.J., Padovan, S., Peale, S.J., Perry, M.E., Smith, D.E., Zuber, M.T. (2013) - The curious case of Mercury's internal structure. J. Geophys. Res. Planets, 118, 1204–1220.

Jarosewich, E. (1990) - Chemical analyses of meteorites: A compilation of stony and iron meteorite analyses. Meteoritics, 25, 323–337.

Lark, L.H., Parman, S., Huber, C., Parmentier, E.M., Head, J.W. (2022) - Sulfides in Mercury's mantle: implications for Mercury's interior as interpreted from moment of inertia. Geophys. Res. Lett., 49, e2021GL096713.

McCubbin, F.M., Riner, M.A., Vander Kaaden, K.E., Burkemper, L.K. (2012) - Is Mercury a volatile-rich planet? Geophys. Res. Lett., 39, L09202.

Namur, O. & Charlier, B. (2017) - Silicate mineralogy at the surface of Mercury. Nat. Geosci., 10, 9–13.

Namur, O., Collinet, M., Charlier, B., Grove, T.L., Holtz, F., McCammon, C. (2016) - Melting processes and mantle sources of lavas on Mercury. Earth Planet. Sci. Lett., 439, 117–128.

Nittler, L.R., Chabot, N.L., Grove, T.L., Peplowski, P.N. (2018) - The chemical composition of Mercury. In: "Mercury: the view after MESSENGER", S.C. Solomon, L.R. Nittler, B.J. Anderson, eds. Cambridge University Press, 30–51.

O'Neill, H.S.C. (2021) - The thermodynamic controls on sulfide saturation in silicate melts with application to ocean floor basalts. In: "Magma redox geochemistry", R. Moretti, D.R. Neuville, eds. John Wiley and Sons, 177–213.

Padovan, S., Wieczorek, M.A., Margot, J.-L., Tosi, N., Solomon. S.C. (2015) - Thickness of the crust of Mercury from geoid-to-topography ratios. Geophys. Res. Lett., 42, 1029–1038.

Pirotte, H., Cartier, C., Namur, O., Pommier, A., Zhang, Y., Berndt, J., Klemme, S., Charlier, B. (2023) - Internal differentiation and volatile budget of Mercury inferred from the partitioning of heat-producing elements at highly reduced conditions. Icarus, 405, 115699.

Pommier, A., Tauber, M.J., Pirotte, H., Cody, G.D., Steele, A., Bullock, E.S., Charlier, B., Mysen, B.O. (2023) - Experimental investigation of the bonding of sulfur in highly reduced silicate glasses and melts. Geochim. Cosmochim. Acta, 363, 114–128.

Riel, N., Kaus, B.J.P., Green, E.C.R., Berlie, N. (2022) -MAGEMin, an efficient Gibbs energy minimizer: application to igneous systems. Geochem. Geophy. Geosy., 23, e2022GC010427.

Saracino, F., Charlier, B., Zhang, Y., Lécaille, M., Lin, Y., Namur, O. (2025) - The role of sulfur on the liquidus temperature and olivine-orthopyroxene equilibria in highly reduced magmas. Chem. Geol., 683, 122777.

Saracino, F., Charlier, B., Zhang, Y., Namur, O. (2026) – The crystallization of Mercury's magma ocean and the formation of its primordial mantle structure. Adv. Geochem. Cosmochem., 2(1), 1003.

Schmidt, M.W. & Kraettli, G. (2022) - Experimental crystallization of the lunar magma ocean, initial selenotherm and density stratification, and implications for crust formation, overturn and the bulk silicate Moon composition. J. Geophys. Res. Planets, 127, 5.

Solomatov, V. (2015) - Magma oceans and primordial mantle differentiation. In: "Treatise on geophysics", G. Schubert, ed. 2nd ed., vol. 9, pp. 81–104. Elsevier.

Vander Kaaden, K.E. & McCubbin, F.M. (2015) - Exotic crust formation on Mercury: consequences of a shallow, FeO-poor mantle. J. Geophys. Res. Planets, 120, 195–209.

Walter, M.J. & Presnall, D.C. (1994) - Melting behavior of simplified lherzolite in the system CaO-MgO-Al_2O_3-SiO_2-Na_2O from 7 to 35 kbar. J. Petrol., 35, 329–359.

Wang, Y., Xiao, Z., Xu, R. (2022) - Multiple mantle sources of high-magnesium terranes on Mercury. J. Geophys. Res. Planets, 127, e2022JE007218.

Warren, P.H., Wasson, J.T. (1979) - The origin of KREEP. Rev. Geophys., 17, 73–88.

White, W.M. (2013) - Geochemistry. Wiley-Blackwell, John Wiley & Sons.

Xu, Y., Lin, Y., Wu, P., Namur, O., Zhang, Y., Charlier, B. (2024) - A diamond-bearing core-mantle boundary on Mercury. Nat. Commun., 15, 5061.

Zolotov, M.Yu., Sprague, A.L., Hauck, S.A., Nittler, L.R., Solomon, S.C., Weider, S.Z. (2013) - The redox state, FeO content, and origin of sulfur-rich magmas on Mercury. J. Geophys. Res. Planets, 118, 138–146.